ELSEVIER

Biophysical Chemistry 109 (2004) 281–293

Biophysical Chemistry

www.elsevier.com/locate/bpc

Spectroscopic properties, catalytic activities and mechanism studies of $[(Tp^{Ph})Co(X)(CH_3OH)_m]\cdot nCH_3OH$: bicarbonate dehydration in the presence of inhibitors

Ying-Ji Sun, Lei Z. Zhang, Peng Cheng*, Hua-Kuan Lin, Shi-Ping Yan, Dai-Zheng Liao, Zong-Hui Jiang, Pan-Wen Shen

Department of Chemistry, Nankai University, Tianjin 300071, PR China

Received 9 October 2003; received in revised form 30 November 2003; accepted 2 December 2003

Abstract

Two inhibitor-containing 'half-sandwich' cobalt(II) complexes $[(Tp^{Ph})Co(X)(CH_3OH)_m]\cdot nCH_3OH$ ((Tp^{Ph}) = hydrotris(3-phenylpyrazolyl)borate; **1**: $X^- = N_3^-$, $m=1$, $n=2$; **2**: $X^- = NCS^-$, $m=0$, $n=0$) have been synthesized and used as the catalysts in the bicarbonate dehydration reaction. The structures of **1** and **2** were determined by X-ray diffraction analysis, which shows that N_3^- and NCS^- coordinate to the Co(II) ions of **1** and **2**, respectively, with the Co–N bond lengths of 1.992(6) Å and 1.901(3) Å. The coordination geometries of the Co(II) complexes in solution are five-coordinated trigonal bipyramid as revealed by the spectroscopic measurements. The dehydration kinetic measurements of HCO_3^- are performed by the stopped-flow techniques at pH < 7.9. The apparent dehydration rate constant k_{obs} varies linearly with Co(II) complex and H^+ concentrations, respectively, and the catalytic activity of **2** is lower than that of **1**. The aqua Co(II) complex must be the reactive catalytic species in the catalyzed dehydration reaction and the rate-determining step is the substitution of the labile water molecule by HCO_3^-. The k_{obs} values increase with increasing reaction temperature, and the large negative entropy of activation also indicates the associative activation mode. The inhibition ability of NCS^- is stronger than that of N_3^-, which can be rationalized by the decreases in the Co–N(N_3^-/NCS^-) bond lengths and effective atomic charges of the Co(II) ions based on the X-ray crystallographic data and theoretical calculations in this work.

Keywords: Spectroscopy; Homogeneous catalysis; Cobalt(II) complex; Inhibitor; Crystal structure; Quantum chemical calculation

1. Introduction

The study of protein–ligand interactions has become a recent hot topic in the fields of biophysical chemistry and enzyme chemistry [1–4]. Advances in the elucidation of structures and dynamic behaviors of protein–ligand complexes have had a dramatic impact on the drug discovery process. Remarkable progress in this area includes the mechanistic investigation of the interactions of a protein–drug complex by Zewail and co-workers that the reduction of drug molecule daunomycin radicals is fundamentally responsible for the enhancement of drug cytotoxicity, which realized

*Corresponding author. Fax: +86-22-23502458.
E-mail address: pcheng@nankai.edu.cn (P. Cheng).

0301-4622/04/$ - see front matter © 2003 Elsevier B.V. All rights reserved.
doi:10.1016/j.bpc.2003.12.001

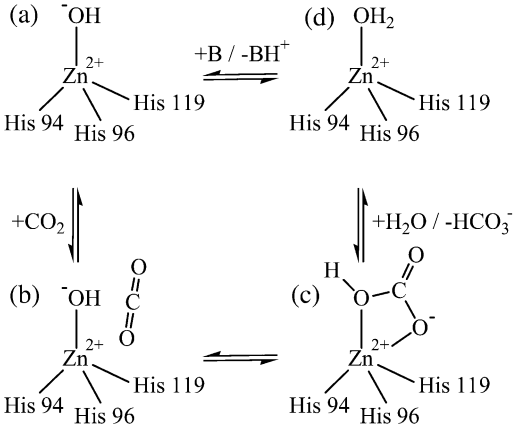

Fig. 1. Schematic representation of the catalytic mechanism for the human CA II catalyzed CO_2 hydration and HCO_3^- dehydration.

the possibility of explaining detailed molecular dynamics of protein–drug interactions [5]. There have also been major research efforts to develop drug candidates as inhibitors for different target proteins, especially carbonic anhydrase (CA) [6–9]. CA catalyzes the diffusion-controlled hydration of carbon dioxide to bicarbonate, which is common in archaeo- and eubacteria, algae, green-plant and animals [10–15]. Being a prototype, detailed studies reveal that the active site of human CA II contains a zinc atom, which is tetrahedrally coordinated by three histidine residues (His-94, His-96, and His-119) and a water molecule/hydroxide ion [16]. The active form of CA is basic, with hydroxide bound to the Zn(II) ion (Fig. 1a). This strong nucleophile attacks the CO_2 molecule bound in a hydrophobic pocket in its neighborhood (Fig. 1b), leading to the formation of bicarbonate coordinated to the Zn(II) ion (Fig. 1c). The bicarbonate ion is then displaced by a water molecule and liberated into solution, resulting in the acid form of the enzyme (Fig. 1d), which is catalytically inactive. In order to regenerate the basic form of CA, a proton transfer reaction from the active site to the environment takes place. It is noteworthy that several groups recently discover that the active site of certain β-CAs contains the Cys_2His-(H_2O or Asp) tetrad ligation environment, providing interesting examples of the convergent evolution of distinct catalytic sites required for the same CO_2 hydration reaction [17,18].

CA is inhibited primarily by two main classes of compounds: the metal complexing small inorganic anions and the unsubstituted sulfonamides possessing the general formula RSO_2NH_2 (R = aryl, hetaryl, perhaloalkyl) [6–9]. The first type of inhibitor was important for understanding the detailed catalytic and inhibitory mechanisms, whereas the second led to the development of several classes of pharmacological agents. Inhibitors of CA can influence fluid dynamics in the eye and be useful in the treatment of glaucoma. Most recently, Supuran and colleagues have successfully prepared the sulfonamide CA inhibitors as long-lasting topically acting antiglaucoma agents [19–22]. Inhibitors of both types directly bind to the metal ion within the enzyme active site, either by substituting the non-protein zinc ligand, such as sulfonamides in deprotonated state, or adding to the metal coordination sphere, which is often the case of inorganic anions that bind to the metal ion as trigonal-bipyramidal adducts. Despite of numerous papers in recent years focusing on the investigation of structure and properties of the sulfonamide inhibitors [19–27], studies concerning the kinetic properties of CA and its model complexes containing different inorganic ions are relatively few.

In this paper, we synthesized two CA model complexes and performed their kinetic measurements in the presence of inhibitors. It is our intention of rationalizing the difference in inhibition ability between two inorganic ions. To well mimic CA, we choose Trofimenko's hydrotris(pyrazolyl)borate ligand system (Tp^R) to synthesize the model complexes [28–30]. The trigonally capping Tp^R has the advantage over other ligand systems in mimicking the coordination environment of CA made by three histidine residues [28–32]. We have, therefore synthesized two inhibitor-containing 'half-sandwich' cobalt(II) complexes $[(Tp^{Ph})Co(X)(CH_3OH)_m]\cdot nCH_3OH$ ((Tp^{Ph}) = hydrotris(3-phenylpyrazolyl)borate; **1**: $X^- = N_3^-$, $m = 1$, $n = 2$; **2**: $X^- = NCS^-$, $m = 0$, $n = 0$), which are very suitable for spectroscopic analysis by using stopped-flow techniques. The paper is organized as follows: the preparation and physical char-

acterization of the cobalt(II) complexes, X-ray crystallographic analysis, dehydration kinetic measurements, and theoretical calculation procedures are described in Section 2. The detailed discussion of the experimental results and explanations of the dehydration kinetics of HCO_3^- catalyzed by the Co(II) complexes are presented in Section 3. A final summary appears in Section 4.

2. Materials and methods

2.1. Starting materials and physical measurements

All the starting chemicals used in this work were of analytical reagent and used without further purification, unless otherwise stated. Hydrotris(3-phenylpyrazolyl)-borate (Tp^{Ph}) was prepared according to the synthetic methodology developed by Eichhorn et al. [33]. The purity of Tp^{Ph} was confirmed by IR, MS-FAB, and elemental analysis. The indicator bromocresol purple (Sigma) and the biological buffer Tris (tris(hydroxymethyl)aminomethane, Sigma) were purchased and used as received. All solutions were prepared using double distilled water that was boiled for more than two hours prior to use to remove the dissolved CO_2. The concentrations of the indicator, Tris, and $NaClO_4$ were kept at 2.5×10^{-4} M, 7.0×10^{-2} M, and 7.5×10^{-2} M, respectively. The pH titration technique was carried out according to the previous published literature procedure [34,35].

Elemental analyses for C, H and N were carried out on a Perkin–Elmer analyzer at the Institute of Elemento-Organic Chemistry, Nankai University. Infrared spectra on KBr pellets were recorded on a Shimadzu IR-408 spectrophotometer in the range of 4000–600 cm^{-1}. UV–Vis spectra in methanol solution were recorded on a Shimadzu UV-2101 spectrophotometer in the 220–800 nm range. Mass spectrum was performed at the Central Laboratory of Nankai University on VG ZAB-HS spectrometer.

*2.2. Synthesis of the compound **1***

$Co(ClO_4)_2\cdot6H_2O$ (73.2 mg, 0.2 mmol) in methanol (5 ml) was added dropwise to methanol (10 ml) containing $K(Tp^{Ph})$ (95.9 mg, 0.2 mmol). The mixture was stirred at room temperature for 10 h. Then, NaN_3 (39.0 mg, 0.6 mml) dissolved in the minimum water was added to the above mixture, and stirred for another 10 h. Purple single crystals of **1** suitable for X-ray diffraction analysis were obtained from slow evaporation of the filtrate. Yield: 99.6 mg (78%). IR (KBr pellet): 2490 (B–H), 2100 (N≡N) cm^{-1}. Anal. for **1**, Calcd for $C_{30}H_{34}BCoN_9O_3$: C, 56.44; H, 5.33; N, 19.74. Found: C, 56.11; H, 5.39; N, 19.35.

*2.3. Synthesis of the compound **2***

The same procedure used for **1** was employed. From $Co(ClO_4)_2\cdot6H_2O$ (73.2 mg, 0.2 mmol), $K(Tp^{Ph})$ (95.9 mg, 0.2 mmol) and KSCN (58.2 mg, 0.6 mmol) was obtained **2**. Purple single crystals suitable for X-ray diffraction analysis were obtained from slow evaporation of the filtrate. Yield: 94.9 mg (85%). IR (KBr pellet): 2475 (B–H), 2050 (C≡N) cm^{-1}. Anal. for **2**, Calcd for $C_{28}H_{22}BCoN_7S$: C, 60.26; H, 3.94; N, 17.56. Found: C, 60.25; H, 3.96; N, 17.55.

*2.4. X-Ray crystallographic analyses for **1** and **2***

Single-crystal X-ray diffraction measurements for **1** and **2** were made at 293(2) K on a Bruker SMART 1000 CCD diffractometer, with graphite-monochromated Mo–Kα radiation ($\lambda=0.71073$ Å), operating in $\omega-2\theta$ scanning mode. Cell parameters were determined from a least-squares refinement. SMART software is used for collecting frames of data, indexing reflections, and determination of lattice constants; SAINTPLUS for integration of intensity of reflections and scaling; SADABS for empirical absorption correction [36]. The structure was solved by direct methods using SHELXS-97 [37], and refined by the full-matrix least-squares method on F^2 using SHELXL-97 [38]. All non-hydrogen atoms were refined anisotropically, while hydrogen atoms were set in calculated positions and treated as riding atoms with a common fixed isotropic thermal parameter. The final cycle of the refinement gives $R=0.0767$ and $R_w=0.1149$ for **1** and $R=0.0434$ and $R_w=0.0941$ for **2**. Crystal data and details of data collection

and structural refinement are given in Table 1. Tables 2 and 3 list the significant bond lengths and distances of **1** and **2**, respectively. Crystallographic data (excluding structure factors) for the structures reported in this paper have been deposited with the Cambridge Crystallographic Data Centre as supplementary publication nos. CCDC-185 567 and 185 568. Copies of the data can be obtained free of charge on application to CCDC, 12 Union Road, Cambridge CB2 1EZ, UK (Fax: +44-1223/336-033; E-mail: deposit@ccdc.cam.ac.uk).

2.5. Dehydration kinetic measurements

All kinetic measurements were made with a Union Giken RA-401 stopped-flow spectrophotometer equipped with a Union Giken RA-451 rapid-scan attachment in order to determine the change in absorption of the reaction mixture directly after mixing under a certain light wavelength. To increase the solubility of the cobalt(II) complexes, 70% ethanol/H_2O (V/V) mixed solution was used. Temperature was maintained by using a Union Giken RA-454 superthermostat, and temperature accuracy is within 0.1 K. The pH values in this work were all directly measured by means of a Beckman Φ71 pH meter. The ionic strength of all test solutions was adjusted to 0.11 M with the aid of $NaClO_4$ for the dehydration reaction. HCO_3^- solutions (7.5×10^{-3} M) were freshly prepared from $NaHCO_3$ and used within 10 h. The most appropriate pH value and light wavelength to study the reaction for this buffer-indicator pair (Tris with bromocresol purple) are ca. 7.0 nm and 595 nm, respectively, which are revealed by UV–Vis absorption spectra. Therefore, the reaction is monitored at 595-nm wavelength with a tungsten lamp as the light source. The apparent first-order dehydration rate constants (k_{obs}^{d}) were obtained with at least three half-lives and represent the average of the best three runs. Reproducibility of the values of k_{obs}^{d} was better than $\pm5\%$.

2.6. Theoretical calculations

During the dehydration process of HCO_3^-, the nucleophilic attack of the free HCO_3^- on the Co(II) ion of the model complex is affected by the effective atomic charge of the Co(II) ion. To obtain information on the variations in the effective atomic charge of the Co(II) ion by coordinating different inhibitors (N_3^-/NCS^-), we have carried out theoretical calculations of **1** and **2** at the UHF level. The basis set consists of the 6-31G** basis functions for H, B, C, N, O, and S [39] and the Los Alamos effective core potential (ECP) for the innermost core electrons of Co with the outermost core electrons included in the valence description, and double-zeta quality description for the valence electrons [40]. Considering the Mulliken population analysis is very dependent on the basis set used, we have performed a NBO population analysis, which works better in these cases. The geometric parameters employed in the calculations were based on the X-ray crystallographic data in this work. All calculations were carried out using the Gaussian-98 package [41].

3. Results and discussion

3.1. Syntheses and structures of the model complexes

A rational approach toward obtaining synthetic analogues of the active site of CA is to use tridentate ligands, such as hydrotris(pyrazolyl)-borate ligand (Tp^R), in which three pyrazolyl groups are attached to a common tetrahedral or trigonal pyramidal center mimicking the active site of the composition $(His)_3Zn{-}OH_2$, where $(His)_3$ are three histidine residues [28–32]. We employed here the effective procedure developed by Eichhorn et al. to synthesize the Tp^R ligand [33]. However, it should be noted that $(Tp^R)_2M(II)$, octahedral full sandwich metal complexes with Tp^R ligands, are easily formed. With the aim to obtain 'half-sandwich' complexes, the phenyl ring, a bulky substituent, has been used here. The purpose of determining the crystal structures of the CA model complexes is two-fold. However, one can gain a deeper insight into the structure-property relations and draw a comparison between

Table 1
Crystallographic data for **1** and **2**

Compound	**1**	**2**
Formula	$C_{30}H_{34}BCoN_9O_3$	$C_{28}H_{22}BCoN_7S$
fw	638.40	558.33
Crystal size/mm^3	0.30×0.15×0.05	0.30×0.10×0.05
Crystal system	triclinic	monoclinic
Space group	*P*-1	$P2_{1/n}$
a/Å	11.004(2)	9.4604(7)
b/Å	11.574(2)	20.1360(16)
c/Å	13.759(3)	13.9450(11)
α/°	80.93(3)	90
β/°	88.78(3)	96.493(2)
γ/°	70.78(3)	90
V/Å^3	1633.3(6)	2639.4(4)
Z	2	4
F (000)	666	1148
ρ(calcd)/Mg m^{-3}	1.298	1.405
μ/mm^{-1}	0.570	0.761
θ range/°	2.55–25.03	1.78–25.03
Reflections collected	5827	10 904
Independent reflections	5330 (R_{int}=0.0692)	4662 (R_{int}=0.0489)
R^a [$I>2\sigma(I)$]	0.0767	0.0434
$R_w{}^b$ [$I>2\sigma(I)$]	0.1149	0.0941
Goodness of fit	0.892	0.969

[a] $R=\sum||F_o|-|F_c||/\sum|F_o|$.
[b] $R_w=\{\sum[w(F_o^2-F_c^2)^2]/\sum[w(F_o^2)^2]\}^{1/2}$.

the structural details of CA and its mimics; however, the crystallographic data obtained from X-ray diffraction analysis can be used in the subsequent theoretical calculations.

Single crystals of **1** and **2** are carefully grown their molecular structure diagrams are shown in Figs. 2 and 3, respectively. In general, **2** shows a pseudo-C_{3v} symmetry, while **1** doesn't rigorously show such a symmetry. In Fig. 2, the coordination geometry about the Co(II) ion center is best described as a trigonal bipyramid formed by three nitrogen atoms of Tp^{Ph}, one nitrogen atom of N_3^-, and one oxygen atom of the methanol molecule. N(1) and O(1) atoms occupies the axial positions, with the N(1)–Co(1)–O(1) bond angle of 170.1(2)°. The Co(1)–N(1) and Co(1)–O(1) bond lengths are 2.133(6) Å and 2.091(5) Å, respectively. This coordination environment of the Co(II) ion is quite similar to that of the five-coordinated adduct of the active site of CA as shown in Section 1. The average Co–N(Tp^{Ph}) bond length is 2.09 Å, which is comparable with 2.11 Å in CA. The Co–N(N_3^-) bond length is 1.992(6) Å.

As shown in Fig. 3, the Co(II) ion is coordinated to three nitrogen atoms of Tp^{Ph} and one nitrogen atom of NCS^- forming a tetrahedron geometry. The N(7)–Co(1)–N(1), N(7)–Co(1)–N(3), and N(7)–Co(1)–N(5) bond angles are 121.94(12)°, 116.70(12)°, and 126.84(12)°, respectively. This coordination environment of the Co(II) ion is consistent with the active site of CA with no coordinated water molecules. The average bond length of Co–N(Tp^{Ph}) is 2.02 Å, being a bit shorter than that of 2.09 Å in 1. The Co–N(NCS^-) bond length is 1.901(3) Å. It is evident from the crystal structures of these two model complexes that the bulky phenyl substituents ensure the syntheses of 'half-sandwich' cobalt(II) complexes. However, the bulky phenyl ring may act as a two-edged sword. Since its size is so big, the dehydrations of HCO_3^- catalyzed by (Tp^{Ph})Co(X) should be rela-

Table 2
Selected bond lengths (Å) and angles (°) of **1**

Co(1)–N(1)	2.133(6)
Co(1)–N(2)	2.062(6)
Co(1)–N(3)	2.086(6)
Co(1)–N(7)	1.992(6)
Co(1)–O(1)	2.091(5)
O(1)–C(10)	1.406(8)
N(7)–N(8)	1.175(8)
N(8)–N(9)	1.147(8)
B(1)–N(6)	1.530(11)
B(1)–N(5)	1.535(11)
B(1)–N(4)	1.578(10)
N(7)–Co(1)–N(2)	120.1(3)
N(7)–Co(1)–N(3)	147.3(3)
N(2)–Co(1)–N(3)	92.6(2)
N(7)–Co(1)–O(1)	88.6(2)
N(2)–Co(1)–O(1)	93.3(2)
N(3)–Co(1)–O(1)	88.1(2)
N(7)–Co(1)–N(1)	96.4(2)
N(2)–Co(1)–N(1)	91.6(2)
N(3)–Co(1)–N(1)	83.1(2)
O(1)–Co(1)–N(1)	170.1(2)
C(10)–O(1)–Co(1)	133.8(5)
N(8)–N(7)–Co(1)	138.8(6)
N(9)–N(8)–N(7)	177.8(9)
N(6)–B(1)–N(5)	109.2(7)
N(6)–B(1)–N(4)	107.6(7)
N(5)–B(1)–N(4)	107.6(7)

tively less efficient than those catalyzed by $(Tp^R)Co(X)$ with small substituents.

3.2. IR and UV–Vis spectroscopies

In the IR spectra on KBr pellets, the typical stretch frequency of ν(B–H) in the free ligand lies at 2430 cm^{-1} and is blue-shifted to 2490 cm^{-1} and 2475 cm^{-1} in **1** and **2**, respectively. This phenomenon is consistent with those observed in other cobalt(II) complexes with hydrotris(pyrazolyl)borate ligands [42]. The stretch frequencies of ν(N≡N) and ν(C≡N) centered at 2100 cm^{-1} and 2050 cm^{-1}, respectively. Other absorption peaks appeared in the range of 1700–600 cm^{-1} can be assigned to the ligand Tp^{Ph}.

The UV–Vis absorption spectra of **1** and **2** have been recorded in methanol solution at room temperature. Board absorption bands have been observed below 400 nm in both cobalt(II) complexes. These bands show strong absorbance and should be assigned to the intraligand absorption. Fig. 4 shows the normalized absorption spectra of **1** and **2** in the visible region in methanol solution at ambient temperature. The intensities of the absorption bands in the visible range are much weaker than those in the ultraviolet range. Dominated absorption bands centered at ca. 560 nm have been observed in both compounds, which are due to the spin-allowed *d*–*d* transitions of the cobalt(II) ions. Seen from the figure, it seems that the *d*-orbital electron absorption of **1** is more markedly influenced by the onset of the intraligand absorption than that of **2**. Other absorption bands in this range are also identified and can be best assigned to the *d*–*d* transitions of the central ions as well, but are relatively weak, which may due to the spin-forbidden nature of some transitions. The absorption spectra of **1** and **2** here show evidence that the coordination spheres of the Co(II) ions in solution are both trigonal bipyramid completed by another solvent molecule, which is different from the coordination mode of the Co(II) ions in the solid state as revealed by the crystallographic analysis.

Table 3
Selected bond lengths (Å) and angles (°) of **2**

Co(1)–N(1)	2.021(3)
Co(1)–N(3)	2.021(3)
Co(1)–N(5)	2.011(3)
Co(1)–N(7)	1.901(3)
S(1)–C(10)	1.597(4)
N(7)–C(10)	1.170(4)
N(2)–B(1)	1.551(5)
N(4)–B(1)	1.547(5)
N(6)–B(1)	1.532(5)
N(7)–Co(1)–N(5)	126.84(12)
N(7)–Co(1)–N(3)	116.70(12)
N(5)–Co(1)–N(3)	95.07(11)
N(7)–Co(1)–N(1)	121.94(12)
N(5)–Co(1)–N(1)	93.75(11)
N(3)–Co(1)–N(1)	95.22(11)
C(10)–N(7)–Co(1)	169.3(3)
N(7)–C(10)–S(1)	179.4(4)
N(6)–B(1)–N(4)	109.4(3)
N(6)–B(1)–N(2)	109.9(3)
N(4)–B(1)–N(2)	107.4(3)

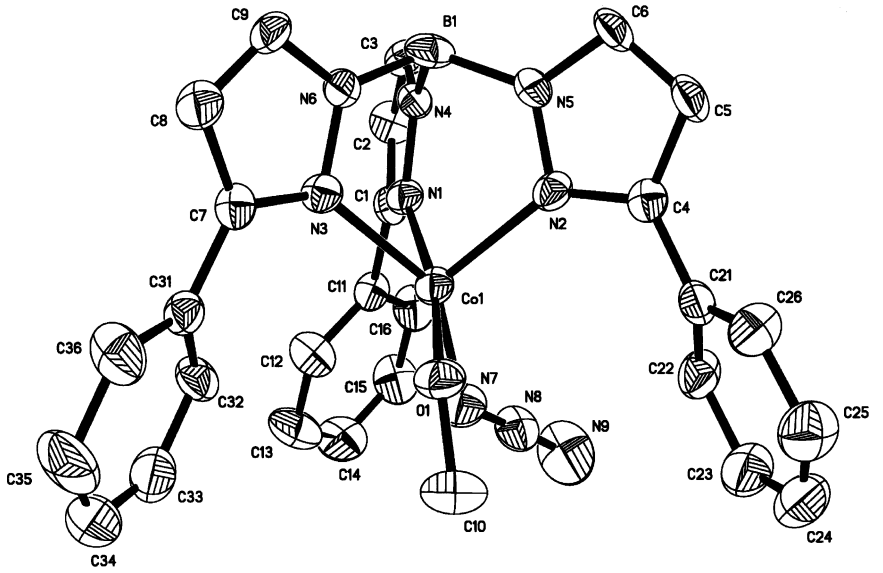

Fig. 2. The molecular structure diagram (30% probability) of **1**. Hydrogen atoms are omitted for clarity.

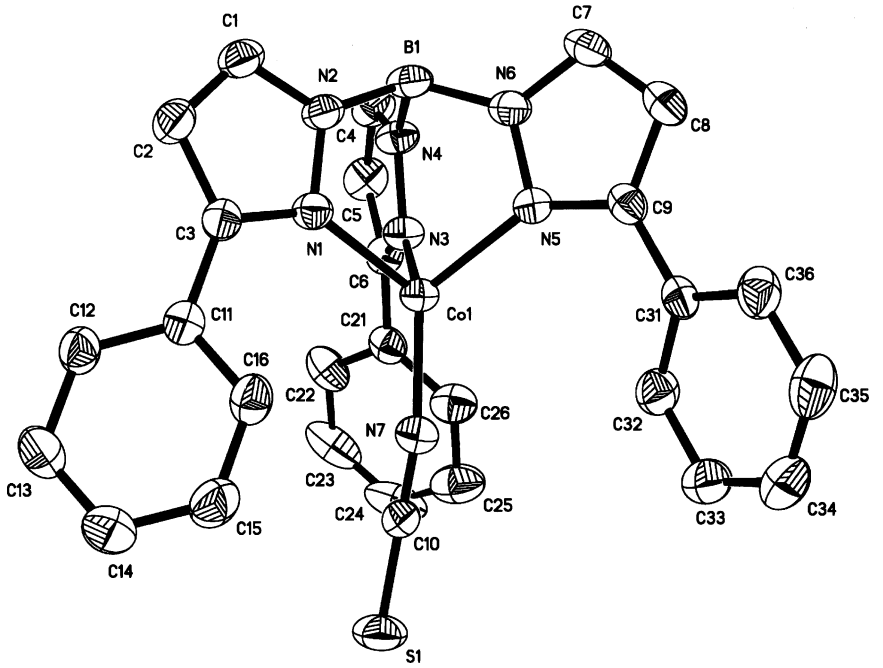

Fig. 3. The molecular structure diagram (30% probability) of **2**. Hydrogen atoms are omitted for clarity.

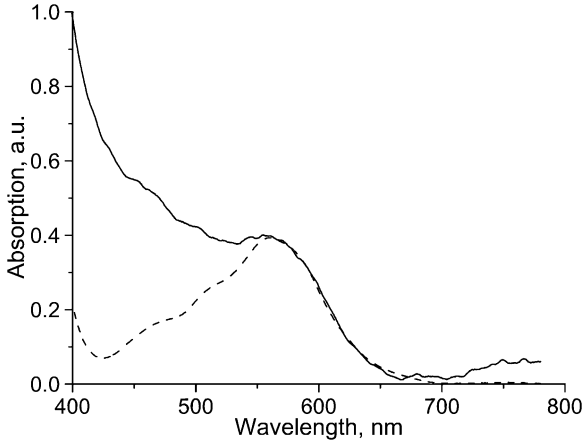

Fig. 4. The normalized absorption spectra of **1** (solid line) and **2** (dashed line) in the visible region in methanol solution at room temperature.

3.3. Kinetics of HCO_3^- dehydration

The acid–base behavior of the title compounds in 0.1 mol l^{-1} $NaNO_3$ at 298 K has been investigated through pH titration. From the titration curve of the Tp^{Ph}-Co binary system we can establish that two H_2O-adducted species $LCoOH_2^+$ and LCoOH are formed in the pH range of 6–8 as shown below (L = the ligands Tp^{Ph} and inhibitor X^-). The two complexes dissociate protons in slightly

$$LCoOH_2^+ \rightleftharpoons LCoOH + H^+ \quad (1)$$

alkaline solution. The pK_a values of **1** and **2** are 7.9 and 7.8, respectively. The lower pK_a value of **2** than **1** may be correlated with a decrease of the effective atomic charge of the cobalt(II) ions, which facilitates the protonation of the water molecules that coordinate to the Co(II) ions. We therefore attribute this protonation to the coordinated water molecule. The catalytic activity of Co(II) complexes is characterized by the pK_a value. The dehydration kinetic measurements of HCO_3^- should be carried out in the case of pH < pK_a to avoid the interference of the reverse hydration reaction especially at higher pH.

As mentioned in Section 2, remarkable changes in absorption spectra were observed in our dehydration kinetics measurements when HCO_3^- was added to the reaction mixture, whereas the hydrogen ion concentration was maintained constant by means of buffer solutions. Measurement of the steady-state absorption spectra of **1** and **2** before and after the addition of HCO_3^- in the buffer-indicator pair (Tris with bromocresol purple) solution shows that the 595 nm absorption changes remarkably, which realizes the performance of the kinetics measurements by monitoring the variation of the absorption. That is, the dehydration rate V can be obtain by the measurement of $dA/\varepsilon dt$.

Under our experimental conditions, the dehydration rate increases linearly with the increase of $[HCO_3^-]$. This means the dehydration is first-order in $[HCO_3^-]$, which indicates that the dehydration rate follows the rate law

$$V = -d[HCO_3^-]/dt = k_{obs}[HCO_3^-] \quad (2)$$

where k_{obs} is the apparent first-order dehydration rate constant. k_{obs} should include all the catalytic species, such as the cobalt(II) complexes, acid and some other species. Therefore, k_{obs} can be written in the following form (complex = Co(II) complex)

$$k_{obs} = k_{cat}[complex]^m + k_H[H^+]^n \quad (3)$$

where k_{cat} and k_H are the catalytic rate constants of the cobalt(II) complex and H^+, respectively, and m and n are constants.

When the observed apparent dehydration rate constants are plotted against the complex concentration at a given pH, we can obtain the values of k_{cat} and m. Typical kinetic traces observed for different concentrations of **1** and **2** catalyzed dehydration of HCO_3^- at pH 7.014 ($\approx$7.0, the most appropriate pH value to study the reaction as denoted in Section 2) are shown by the plot of k_{obs} vs. [complex] in Fig. 5. It is evident that the apparent dehydration rate constants k_{obs} vary linearly with the total complex concentrations showing a first-order dependence on cobalt(II) complex ($m = 1$). Regression of k_{obs} vs. [complex] for the two complexes, from the slope, we have

$k_{cat} = 135\ M^{-1}\ s^{-1}$ for **1**

$k_{cat} = 70.4\ M^{-1}\ s^{-1}$ for **2**

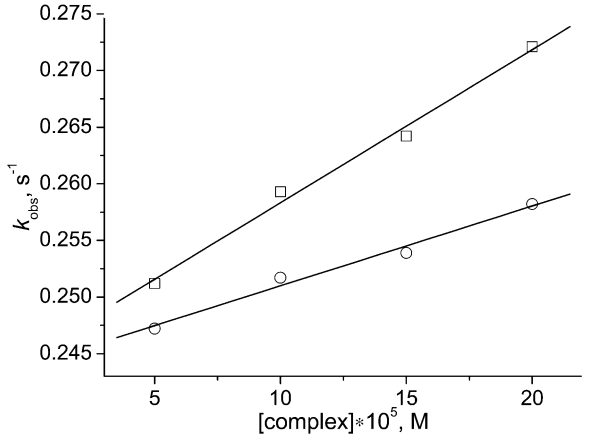

Fig. 5. Plot of k_{obs} vs. [complex] for the dehydration of HCO_3^-. Experimental conditions: pH 7.014; [$NaHCO_3$] = 7.5×10^{-3} M; ionic strength = 0.11 M; [buffer] = 7.0×10^{-2} M; [indicator] = 2.5×10^{-4} M; temperature = 25.0 °C. Key: (□) **1**; (○) **2**. The sold line is the best linear fitting of the data.

The catalytic activity of **2** is lower than **1** indicating that the inhibition ability of the inorganic ion NCS^- is stronger than that of N_3^-. The effect of free Co(II) ions on the reaction was also checked at the same pH value, but no catalysis was observed.

In Fig. 5, the intercept values are not equal to zero, which means that in the absence of the cobalt(II) complexes, the dehydration reactions also take place. That is, H^+ and/or solvent can catalyze HCO_3^- dehydration. Plot of k_{obs} vs. different $[H^+]$ at a typical complex concentration and in the absence of the Co(II) compounds is shown in Fig. 6. It is evident that first-order dependence on $[H^+]$ has been observed ($n=1$). Linear fitting of the data gives nearly the same k_H value indicating the reliability of our kinetic measurement. The mean value of k_H is 8.82×10^5 M^{-1} s^{-1}. It is noticeable that the intercept is not zero in Fig. 6, which shows that besides k_H, there is a slow reaction with $k_0=0.152$ s^{-1}. The small value of k_0 is probably due to the solvolysis of bicarbonate. This means that HCO_3^- can be hydrolyzed by solvolysis, but the reaction rate is low. The kinetic measurement data in Figs. 5 and 6 also show consistency, which has been confirmed by cross-check. From the above results, it has been found that the reaction rate is of first-order with respect to cobalt(II) complex and hydrogen ion concentrations. Therefore, we have the following kinetic equation

$$V = k_{obs}[HCO_3^-] = (k_{cat}[complex] + k_H[H^+] + k_0)[HCO_3^-] \quad (4)$$

The activation parameters for the catalyzed dehydration reaction were determined from the temperature dependence of the k_{obs} values. The temperature dependent dehydration reaction rate constants are measured at 298 K and 310 K, respectively. The measurement results show that the k_{obs} values increase with increasing reaction temperature (for **1**: from 0.264 to 0.286 s^{-1}; for **2**: from 0.254 to 0.279 s^{-1}), which is consistent with the enzyme catalytic behavior. From the Eyring Eq. (5) and the Arrhenius Eq. (6)

$$\ln(k/T) = -\Delta H_m^{\neq}/RT + \Delta S_m^{\neq}/R + \ln(R/N_a h) \quad (5)$$

$$\ln(k_2/k_1) = E_a(T_2 - T_1)/RT_1T_2 \quad (6)$$

where the symbols have their usual meaning. The

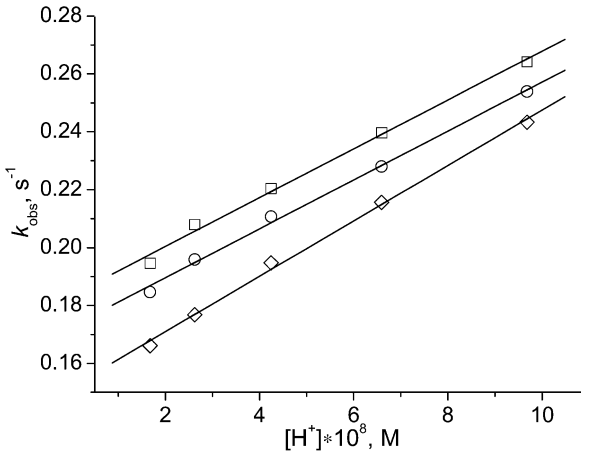

Fig. 6. Plot of k_{obs} vs. $[H^+]$ for the dehydration of HCO_3^-. Experimental conditions: [complex] = 1.5×10^{-5} M; [$NaHCO_3$] = 7.5×10^{-3} M; ionic strength = 0.11 M; [buffer] = 7.0×10^{-2} M; [indicator] = 2.5×10^{-4} M; temperature = 25.0 °C. Key: (□) **1**; (○) **2**; (◇) in the absence of Co(II) complexes. The sold line is the best linear fitting of the data.

Table 4
The activation parameters $\Delta H_m^{\neq}$ (kJ mol^{-1}), $\Delta S_m^{\neq}$ (J K^{-1} mol^{-1}), and E_a (kJ mol^{-1})[a]

Compound	$\Delta H_m^{\neq}$	$\Delta S_m^{\neq}$	E_a
1	2.491	−320.3	2.179
2	3.748	−316.5	2.725

[a] Experimental conditions: pH 7.014; [$NaHCO_3$] = 7.5×10^{-3} M; [complex] = 1.5×10^{-5} M; ionic strength = 0.11 M; [buffer] = 7.0×10^{-2} M; [indicator] = 2.5×10^{-4} M.

activation enthalpy $\Delta H_m^{\neq}$, activation entropy $\Delta S_m^{\neq}$, and apparent activation energy E_a are listed in Table 4. Although the activation parameters are often not discriminating factors in recognizing the reaction pathway, the large negative entropy of activation ($\Delta S_m^{\neq}$), however, clearly indicates an associative activation mode. This step may be assigned to the reaction between the aqua Co(II) complex and HCO_3^- during the dehydration process. The apparent activation energy of **1** (2.179 kJ mol^{-1}) is lower than that of **2** (2.725 kJ mol^{-1}), this being the origin of different catalytic properties of the model complexes.

3.4. Mechanisms of HCO_3^- dehydration

As revealed by the UV–Vis absorption spectra, the coordination geometries of the Co(II) ions of **1** and **2** in solution are both trigonal bipyramid completed by another solvent molecule. Therefore, the dehydration reaction of HCO_3^- catalyzed by the Co(II) complexes can be accounted for in terms of the mechanism outlined in Fig. 7, which are based on the principle that only the aqua complex can react with HCO_3^- in order to catalyze the dehydration reaction [6–16]. Seen from this figure, a solvent water molecule coordinates to the Co(II) ion, to complete a five-coordinated aqua complex showing a trigonal bipyramidal geometry. This five-coordinated H_2O-adduct is considered as the reactive catalytic species in the dehydration of HCO_3^-. In this mechanism, it is assumed that the produced bicarbonate complex is unstable and rapidly releases CO_2. It is reasonable to assume that no stable bicarbonate complex is formed since the release of CO_2 was observed during the reaction. In addition, no evidence whatsoever could be found for the presence of such a complex. Hence, the rate-determining step of the dehydration reaction must be the substitution of the labile water molecule by HCO_3^-, which nucleophilic attacks on the Co(II) ion of the model complex. The overall mechanism of dehydration of HCO_3^- catalyzed by the model complexes can be, therefore stated as follows: in the case of $pH < pK_a$, the aqua complex exhibits the catalytic activity on the dehydration of HCO_3^- in which the rate-determining step is the substitution of the labile water molecule by HCO_3^-, followed by the rapid decarboxylation of the coordinated bicarbonate molecule as found for many model bicarbonate complexes [43].

As has been pointed out, the observed apparent dehydration rate constant is of first-order with respect to the total complex concentration

$$k_{obs} = k_{cat}[\text{complex}] + k_H[H^+] + k_0 \quad (7)$$

From the following stoichiometric equation (L = the ligands Tp^{Ph} and inhibitor X^-)

$$[\text{complex}] = [LCoOH_2] + [LCoOH^-] \quad (8)$$

we have

$$[\text{complex}] = [LCoOH_2](1 + K_a/[H^+]) \quad (9)$$

According to the above proposed mechanism,

$$k_{obs} = k_{rds}[LCoOH_2] + k_H[H^+] + k_0 \quad (10)$$

where k_{rds} is the dehydration rate constant of the rate-determining step (rds). Combination of the Eqs. (9) and (10),

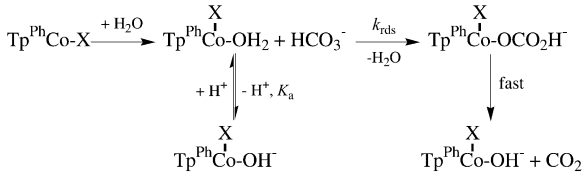

Fig. 7. Suggested mechanism for the dehydration of HCO_3^- catalyzed by the Co(II) complexes (X^- = inhibitor N_3^-/NCS^-).

$$k_{obs} = k_{rds}[complex][H^+]/([H^+] + K_a) + k_H[H^+] + k_0 \quad (11)$$

Comparison of the Eq. (7) and Eq. (11), we, therefore have

$$k_{cat} = k_{rds}[H^+]/([H^+] + K_a) \quad (12)$$

Using the K_a values of **1** and **2** previously obtained by pH titration, we can calculate the dehydration rate constants of the rate-determining step

$k_{rds} = 153\ M^{-1}\ s^{-1}$ for **1**

$k_{rds} = 81.9\ M^{-1}\ s^{-1}$ for **2**

The higher the k_{rds} value, the lower the activation energy barrier. Therefore, the origin of the variation in the inhibition ability between the N_3^- and NCS^- can be correlated with changes in the activation energy barriers of the rate-determining step. The present results have proved that cobalt(II) complex with Tp^{Ph} ligand system can serve as a good CA model that catalyzes the bicarbonate hydrolysis. From k_{cat} and k_{rds} values, we can conclude that different small inorganic ions that coordinated to the Co(II) ions can influence the catalytic activity of their cobalt(II) complexes. This may be due to the variation of the effective atomic charges of the Co(II) ions, which could be verified by theoretical calculations.

3.5. Theoretical calculations of effective atomic charges

It is evident from the above experimental measurements that the inhibition ability of NCS^- is stronger than that of N_3^-. During the dehydration process of HCO_3^-, the nucleophilic attack of the free HCO_3^- on the Co(II) ion of the model complex is affected by the effective atomic charge of the Co(II) ion. In this case, the nitrogen atom of the inhibitor (N_3^-/NCS^-) that coordinates to the Co(II) ion serves as the electron donor. Low effective atomic charges caused by stronger donor inhibitors is disadvantageous to the nucleophilic attack of the free HCO_3^- ion on the Co(II) ion. As far as the single crystal data are concerned, the Co–N(NCS^-) bond length (1.901(3) Å) is shorter than the Co–N(N_3^-) bond length (1.992(6) Å) indicating that the NCS^- ion is more buried than the N_3^- ion. Meanwhile, since the Co–N(NCS^-) bond length is shorter than the Co–N(N_3^-) bond length, the electrons from the N donor atoms of the inhibitor are more delocalized on the Co(II) ion leading to the decrease of the effective atomic charge of the Co(II) ion, which is adverse to the nucleophilic attack of the free HCO_3^- ion on the Co(II) ion.

To obtain detailed information on the variations in the effective atomic charge of the Co(II) ion by coordinating different inorganic ions (N_3^-/NCS^-), we have carried out theoretical calculations of **1** and **2** at the UHF level. The basis set consists of the Los Alamos effective core potential (ECP) for Co with the outermost core orbitals included in the valence description and the 6-31G** basis functions for the other atoms. Since the Mulliken population analysis is very dependent on the basis set used, a natural bond orbital (NBO) population analysis has been performed, which works better in these cases. Based on the crystal data available in the work, the effective atomic charges of the Co(II) ion can be obtained quantitatively by these calculations. Full lists of the results of NBO population analysis can be found in the supporting materials. The charges of the Co(II) ions have been found to be 1.466 and 1.398 for **1** and **2**, respectively. Therefore, we can conclude that the electrons from the N donor atom of the inhibitor NCS^- are more delocalized on the Co(II) ion resulting in the decrease of the effective atomic charge, which can rationalize the variations in inhibition ability between N_3^- and NCS^-.

4. Conclusion

In summary, we have reported here the syntheses, structures, spectroscopic properties, dehydration kinetics and mechanisms of two inhibitor-containing 'half-sandwich' cobalt(II) complexes $[(Tp^{Ph})Co(X)(CH_3OH)_m]\cdot nCH_3OH$ (**1**: $X^- = N_3^-$, $m = 1$, $n = 2$; **2**: $X^- = NCS^-$, $m = 0$, $n = 0$) as the

catalysts in the bicarbonate dehydration reaction. The Co(II) complexes in the kinetic measurements exhibit a catalytic activity for the dehydration of HCO_3^- at pH < 7.9. The coordination spheres of the aqua model complexes are five-coordinated trigonal bipyramid, which is confirmed by the spectroscopic measurements. The apparent dehydration rate constant k_{obs} varies linearly with Co(II) complex and H^+ concentrations, respectively, and the catalytic activity of **2** is evidently lower than that of **1**. The aqua model complex must be the reactive catalytic species in the catalyzed dehydration reaction and the rate-determining step is the substitution of the labile water molecule by HCO_3^-. The k_{obs} values increase with increasing reaction temperature, and the large negative entropy of activation indicates an associative activation mode. The inhibition ability of NCS^- is stronger than that of N_3^-, which can be rationalized by the decreases in the Co–N(N_3^-/NCS^-) bond lengths and effective atomic charges of the Co(II) ions based on the X-ray crystallographic data and theoretical calculations in this work. The results showcased in the present contribution are beneficial to our further investigation and understanding of the detailed dynamic behaviors of HCO_3^- dehydration catalyzed by transition-metal complexes using Tp^R ligand system.

Acknowledgments

The authors thank the financial support from the National Natural Science Foundation of China (Nos. 29971017, 90101028) and the TRAPOYT of MOE, China. The authors truly appreciate the referee for pointing out the relevant publications concerning the Cys_2His-(H_2O or Asp) ligand set of CA.

References

[1] Biophysics Special Issue, Chem Phys Chem 3 (2002) 237–303.
[2] R.E. Babine, S.L. Bender, Molecular recognition of protein–ligand complexes: applications to drug design, Chem. Rev. 97 (1997) 1359–1472.
[3] B.F. Cravatt, E.J. Sorensen, Chemical strategies for the global analysis of protein function, Curr. Opin. Chem. Biol. 4 (2000) 663–668.
[4] A.Y. Louie, T.J. Meade, Metal complexes as enzyme inhibitors, Chem. Rev. 99 (1999) 2711–2734.
[5] D. Zhong, S.K. Pal, C. Wan, A.H. Zewail, Femtosecond dynamics of a drug–protein complex: daunomycin with apo riboflavin-binding protein, Proc. Natl. Acad. Sci. USA 98 (2001) 11 873–11 878.
[6] C.T. Supuran, A. Scozzafava, A. Casini, Carbonic anhydrase inhibitors, Med. Res. Rev. 23 (2003) 146–189.
[7] C.T. Supuran, A. Scozzafava, Applications of carbonic anhydrase inhibitors and activators in therapy, Exp. Opin. Ther. Patents 12 (2002) 217–242.
[8] C.T. Supuran, A. Scozzafava, Carbonic anhydrase inhibitors, Curr. Med. Chem. 1 (2001) 61–97.
[9] C.T. Supuran, A. Scozzafava, Carbonic anhydrase inhibitors and their therapeutic potential, Exp. Opin. Ther. Patents 10 (2000) 575–600.
[10] F. Botre, G. Gros, B.T. Storey, Carbonic Anhydrase, VCH, Weinheim, Germany, 1991.
[11] D.N. Silverman, S. Lindskog, The catalytic mechanism of carbonic anhydrase: implications of a rate-limiting protolysis of water, Acc. Chem. Res. 21 (1988) 30–36.
[12] D.W. Christianson, C.A. Fierke, Carbonic anhydrase: evolution of the zinc binding site by nature and by design, Acc. Chem. Res. 29 (1996) 331–339.
[13] W.N. Lipscomb, N. Sträter, Recent advances in zinc enzymology, Chem. Rev. 96 (1996) 2375–2433.
[14] G. Parkin, The bioinorganic chemistry of zinc: synthetic analogues of zinc enzymes that feature tripodal ligands, Chem. Commun. (2000) 1971–1985.
[15] R.G. Khalifah, Reflections on Edsall's carbonic anhydrase: paradoxes of an ultra fast enzyme, Biophys. Chem. 100 (2003) 159–170.
[16] I. Bertini, C. Luchinat, in: I. Bertini, H.B. Gray, S.J. Lippard, J.S. Valentine (Eds.), Bioinorganic Chemistry, University Science Books, Sausalito, CA, 1994.
[17] M.S. Kimber, E.F. Pai, The active site architecture of Pisum sativum β-carbonic anhydrase is a mirror image of that of α-carbonic anhydrases, EMBO J. 19 (2000) 1407–1418.
[18] S. Mitsuhashi, T. Mizushima, E. Yamashita, M. Yamamoto, T. Kumasaka, H. Moriyama, et al., X-ray structure of β-carbonic anhydrase from the red alga, Porphyridium purpureum, reveals a novel catalytic site for CO_2 hydration, J. Biol. Chem. 275 (2000) 5521–5526.
[19] F. Maestrelli, P. Mura, A. Casini, F. Mincione, A. Scozzafava, C.T. Supuran, Cyclodextrin complexes of sulfonamide carbonic anhydrase inhibitors as long-lasting topically acting antiglaucoma agents, J. Pharm. Sci. 91 (2002) 2211–2219.
[20] A. Scozzafava, L. Menabuoni, F. Mincione, C.T. Supuran, Carbonic anhydrase inhibitors. A general approach for the preparation of water-soluble sulfonamides incorporating polyamino-polycarboxylate tails and of their metal complexes possessing long-lasting, topical intraocular pressure-lowering properties, J. Med. Chem. 45 (2002) 1466–1476.

[21] A. Scozzafava, L. Menabuoni, F. Mincione, G. Mincione, C.T. Supuran, Carbonic anhydrase inhibitors: synthesis of sulfonamides incorporating dtpa tails and of their zinc complexes with powerful topical antiglaucoma properties, Bioorg. Med. Chem. Lett. 11 (2001) 575–582.

[22] M. Ilies, C.T. Supuran, A. Scozzafava, A. Casini, F. Mincione, L. Menabuoni, et al., Carbonic anhydrase inhibitors: sulfonamides incorporating furan-, thiophene- and pyrrole-carboxamido groups possess strong topical intraocular pressure lowering properties as aqueous suspensions, Bioorg. Med. Chem. 8 (2000) 2145–2155.

[23] M. Ferraroni, F. Briganti, W.R. Chegwidden, C.T. Supuran, A. Scozzafava, Crystal analysis adduct of aromatic sulfonamide binding to native and (Zn)2 adduct of human carbonic anhydrase I Michigan 1, Inorg. Chim. Acta 339 (2002) 135–144.

[24] P.A. Boriack-Sjodin, S. Zeitlin, H.H. Chen, L. Crenshaw, S. Gross, A. Dantanarayana, et al., Structural analysis of inhibitor binding to human carbonic anhydrase II, Protein Sci. 7 (1998) 2483–2489.

[25] M. Bulbul, N. Saracoglu, O.I. Kufrevloglu, M. Ciftci, Bile acid derivatives of 5-amino-1,3,4-thiadiazole-2-sulfonamide as new carbonic anhydrase inhibitors: synthesis and investigation of inhibition effects, Bioorg. Med. Chem. 10 (2002) 2561–2567.

[26] O. Arslan, U. Cakir, H.I. Ugras, Synthesis of new sulfonamide inhibitors of carbonic anhydrase, Biochemistry (Moscow) 67 (2002) 1055–1057.

[27] O. Arslan, Inhibition of bovine carbonic anhydrase by new sulfonamide compounds, Biochemistry (Moscow) 66 (2001) 982–983.

[28] S. Trofimenko, Polypyrazolylborates, a new class of ligands, Acc. Chem. Res. 4 (1971) 17–22.

[29] S. Trofimenko, J.C. Calabrese, J.S. Thompson, Novel polypyrazolylborate ligands: coordination control through 3-substituents of the pyrazole ring, Inorg. Chem. 26 (1987) 1507–1514.

[30] S. Trofimenko, Recent advances in poly(pyrazolyl)borate (scorpionate) chemistry, Chem. Rev. 93 (1993) 943–980.

[31] S. Hikichi, M. Akita, Y. Moro-oka, New aspects of the cobalt-dioxygen complex chemistry opened by hydrotris(pyrazoly)borate ligands (Tp^R): unique properties of Tp^RCo-dioxygen complexes, Coord. Chem. Rev. 198 (2000) 61–87.

[32] Y.-J. Sun, W.-Z. Shen, P. Cheng, S.-P. Yan, D.-Z. Liao, Z.-H. Jiang, et al., The first example of half-sandwich cobalt(III) complex with hydrotris(pyrazolyl)borate ligand, Inorg. Chem. Commun. 5 (2002) 512–515.

[33] D.E. Eichhorn, W.H. Armstrong, M{hydrotris(3-phenylpyrazol-l-yl)borate}$_2$: sterically encumbered iron(II) and manganese(II) complexes, Inorg. Chem. 29 (1990) 3607–3612.

[34] S.-R. Zhu, H.-K. Lin, C.-C. Lin, F.-P. Kou, Y.-T. Chen, A convenient method for the synthesis of macrocyclic dioxotetraamine ligands bearing pendent coordinating groups and the properties of their copper(II) complexes, Inorg. Chim. Acta 228 (1995) 225–232.

[35] S.-R. Zhu, F.-P. Kou, H.-K. Lin, C.-C. Lin, M.-R. Lin, Y.-T. Chen, Synthesis of novel macrocyclic polyamines with a pendant phenol group and properties and structures of their copper(II) complexes, Inorg. Chem. 35 (1996) 5851–5859.

[36] G.M. Sheldrick, SADABS, University of Göttingen, Göttingen, Germany, 1996.

[37] G.M. Sheldrick, SHELXS-97, University of Göttingen, Göttingen, Germany, 1997.

[38] G.M. Sheldrick, SHELXL-97, University of Göttingen, Göttingen, Germany, 1997.

[39] M.M. Francl, W.J. Petro, W.J. Hehre, J.S. Binkley, M.S. Gordon, D.J. Defrees, et al., Self-consistent molecular orbital methods. XXIII. A polarization-type basis set for second-row elements, J. Chem. Phys. 77 (1982) 3654–3665.

[40] P.J. Hay, W.R. Wadt, Ab initio effective core potentials for molecular calculations. Potentials for the transition metal atoms Sc to Hg, J. Chem. Phys. 82 (1985) 270–283.

[41] M.J. Frisch, G.W. Trucks, H.B. Schlegel, G.E. Scuseria, M.A. Robb, J.R. Cheeseman, et al., Gaussian 98, Revision A.9, Gaussian, Inc, Pittsburgh, PA, 1998.

[42] A. Hayashi, K. Nkajima, M. Nonoyama, Preparation and structures of cobalt(III) complexes containing hydrotris(pyrazol-1-yl)borate and triamines, Polyhedron 16 (1997) 4087–4095.

[43] D.A. Palmer, R. van Eldik, The chemistry of metal carbonato and carbon dioxide complexes, Chem. Rev. 83 (1983) 651–731.